Three-Dimensional Motion and Perfusion Quantification in Gated Single-Photon Emission Computed Tomograms

Tracy L. Faber, Marvin S. Akers, Ronald M. Peshock, and James R. Corbett

Departments of Radiology and Internal Medicine (Cardiology), University of Texas Southwestern Medical Center, Houston, Texas

Methods for quantification and display of left ventricular (LV) functional parameters from gated single-photon emission computed tomographs are described. Using previously documented surface detection methods, we developed techniques for calculating global variables, such as volumes and areas, as well as local variables such as segmental motion and local perfusion from gated tomographic radionuclide ventriculograms (TRVG) and gated perfusion tomograms (sestamibi). We have developed three-dimensional displays to allow realistic visualizations of the results. The motion results have been validated using correlative magnetic resonance imaging (MRI) studies; motion calculated from user-traced MR images of the heart was compared to motion calculated from automatically detected surfaces in TRVG and sestamibi. The average motion error was calculated to be 0.67 mm in TRVG and −0.21 mm in sestamibi. Errors were largest in basal LV regions; we explain this phenomenon using simulations. Finally, we present additional examples of the analysis using studies obtained from normal volunteers and from subjects whose coronary artery anatomies were known.

J Nucl Med 1991; 32:2311–2317

Recent advances in computer hardware and software have made gated single-photon emission computed tomography (GSPECT) practical. Previous quantitative and semi-quantitative analyses have shown two types of GSPECT images, tomographic radionuclide ventriculograms (TRVG), and gated perfusion tomography with ^{99m}Tc 2-methoxy-isobutyl-isonitrile (sestamibi) to have advantages over two-dimensional or ungated images (*1*, *2*). However, these images are much more difficult to analyze because of the large amount of information contained in them. Quantitative three-dimensional/four-dimensional analysis techniques and improved display of the quantified information should allow better visualizations of left ventricular perfusion, structure, and function.

Received March 4, 1991; revision accepted August 9, 1991

For reprints contact: For reprints contact: James R. Corbett, M.D., The University of Texas Southwestern Medical Center, Department of Radiology, 5323 Harry Hines Blvd., Dallas, TX 75235-9058.

Quantification requires that the LV be segmented from the surrounding regions. We have previously described (*3–6*) a LV surface detector that identifies sets of endocardial and/or epicardial points from TRVG and sestamibi images for all frames of the cardiac cycle. A more robust validation of this algorithm has been reported recently (*7*).

This surface detector, applied to GSPECT images, can be used for quantifying wall motion and perfusion. We describe a three-dimensional motion calculation that is not dependent upon any coordinate system. We use a simulation to analyze the expected errors in quantification of motion and perfusion given the assumptions of the edge detector and show that they are not prohibitive. We validate the automatically calculated motion and perfusion values from GSPECT images by comparing them with those determined from hand-traced surfaces of cardiac rotation MR images of the same patients. Finally, we present several TRVG and sestamibi studies and demonstrate correlations with known coronary anatomy.

MATERIALS AND METHODS

GSPECT Protocols

Radionuclide ventriculography was performed under resting conditions, after the labeling of autologous red blood cells in vitro with 30 mCi of [^{99m}Tc]pertechnetate (*8*). Gated sestamibi imaging was performed following an exercise protocol. Exercise consisted of a symptom-limited maximal upright treadmill test. Patients began exercise with either the Bruce or modified Bruce protocols depending on their level of fitness. Patients beginning with a modified Bruce protocol were advanced into stages of the standard Bruce protocol as tolerated. Exercise was terminated only for progressive chest pain, complex ventricular arrhythmias, progressive hypotension, or excessive fatigue. Sixty to ninety seconds before the termination of exercise, an intravenous injection of 30 mCi/70 kg sestamibi was given. After 15–20 min of recovery, a light meal was provided to accelerate hepatobiliary clearance of the sestamibi. One to 2 hr after injection, tomographic imaging was initiated.

GSPECT Imaging

TRVG images were acquired using a three-detector rotating gamma camera (PRISM, Ohio Imaging, Picker, Highland Hgts, Ohio); sestamibi images were acquired using an Omega 500 Sentinel (Technicare, Solon, Ohio) tomographic camera. Both

were equipped with low-energy, general purpose parallel-hole collimators. Energy discrimination was provided by a 15% window centered over the 140 keV photopeak of ^{99m}Tc. Projections were acquired with the patient in the supine position with the arms positioned beside the head. Each projection was corrected on-line for nonuniformity with a 300 million count flood. A total of 120 gated projection image sets were obtained over 360° for the TRVGs using the closest elliptical orbit. A circular orbit was used to acquire projections for the sestamibi images at 32 equally spaced positions about 180°, from 45° right anterior oblique to 45° left posterior oblique. Each projection image set was acquired at a temporal resolution of 16 frames equally distributed over the entire cardiac cycle using standard gated acquisition software. Each was recorded at a spatial resolution of 64×64 using a dedicated nuclear medicine computer system. Sestamibi gated projection image sets were obtained for a preset time of 60 sec and contained 40,000 to 70,000 counts per frame; TRVG sets were acquired for 25 sec and contained 100,000 to 200,000 counts per frame. Total TRVG imaging time was approximately 17 min; sestamibi imaging time was approximately 30 min.

Reconstruction

Gated tomographic projection image sets were reconstructed into transverse sections using filtered backprojection with a ramp-Butterworth filter of cutoff =.43 and order 4. Neither attenuation nor scatter correction was performed. Only those projections from 45° right anterior oblique to 45° left posterior oblique, 180° total, were reconstructed. Short-axis sections were obtained from the transaxial slices using standard nuclear medicine software. These short-axis sections were used as the input to our surface detector, and therefore, for the quantification of perfusion and motion.

MRI

Magnetic resonance images were acquired from all patients. Patients were imaged using 0.35 Tesla MRI device (Toshiba America, MRI, Inc., South San Francisco, CA) Through use of patient positioning and oblique imaging planes, short-axis sections were obtained (*9*). Spin-echo images were obtained with a repetition time equal to cardiac cycle length and an echo time of 30 msec. The voxel size was 1.7 × 1.7 × 10 mm. Using a repeated multislice or rotation technique (*10*), images were obtained in each slice at 5 points in the cardiac cycle. Data acquisition for the end-diastolic image occurred 40 msec after the R-wave trigger with subsequent images obtained at progressive 100-msec intervals. Hence, images were acquired at end diastole and throughout systole into early diastole. The total time for acquiring the complete set of images was approximately 45 min.

Surface Detection

Details of the surface detector can be obtained in (*3,7*). In essence, we posed the LV surface detection as a labeling problem that could be solved using a relaxation technique. We considered each object to be an angle in the coordinate system shown in Figure 1. Note that this coordinate system can be thought of as cylindrical system for the basal ¾ of the LV, and a spherical system for the apical ¼; similar hybrid coordinate systems have been used for extracting myocardial tracer distributions for perfusion quantification (*11*). The task was then to label each angle in the coordinate system with the radius of the LV surface at that angle. The method required an initial estimate of how likely the occurrence of an edge point was at each radius and how the radii

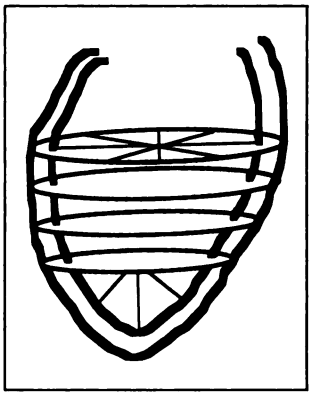

FIGURE 1. Coordinate system used to determine LV surface points. A cylindrical coordinate system is used for the basal ¾ of the LV; nine contours containing 216 points are detected. An additional 72 points are found using a spherical coordinate system in the apical LV region. Points are detected on both the endocardial and epicardial surfaces, for each of 16 time frames.

of neighboring angles' surface points were related. We used image intensity gradients to estimate the initial likelihoods, where a high gradient indicated a high likelihood of the surface point occurring at that radius. Relationships between the radii of neighboring surface points were determined using a set of normal GSPECT studies to describe the shape of the LV based only on how surface point radii differed from angle to angle. In general, differences in radii between neighboring angles were determined to be small. Based on the initial likelihoods and the neighborhood relationships, we could apply a relaxation labeling technique to iteratively revise the initial likelihoods of each radius of each surface point according to how that radius differed from that of its neighbors. Any radius with a high image intensity gradient would start out with a high likelihood of being on the LV surface, but would only remain so if neighboring angles also had high likelihood radii of similar lengths. Low likelihood surface points could become high-likelihood surface points if they were surrounded by neighboring angles with similar-length high-likelihood surface points. Thus, the surface points were estimated initially based on image gradients, but were revised based on knowledge of the expected shape of the LV.

In practice, the user was asked to identify the LV long axis; otherwise, the method was entirely automatic. Twenty-four points were detected in nine contours perpendicular to this axis. The ¾ point of the long-axis, where the cylindrical system was abandoned in favor of the spherical system, served as the origin for the spherical coordinate system. Seventy-two points around three latitude lines and 24 longitude lines were detected in the apical region using the spherical system. Thus, 288 points were detected on both the endocardial and epicardial surfaces for each time frame. The total time required for this surface detection varied, but required approximately 3 min for blood-pool studies, and 4–6 min for sestamibi studies.

Quantification of Motion and Perfusion

Global variables, such as volumes, ejection fraction, and myocardial mass were computed by connecting the surface points of each frame into triangles to form a polygonal solid. The volume of the solid could be computed; thus endocardial and epicardial volumes were known for all time frames. The end-diastolic (ED) and end-systolic (ES) frames were determined from the volumes; the ejection fraction was computed using this information.

Local measurements were also made using these triangulated surfaces. Perfusion was quantified using the ED frame by computing the maximum pixel counts between the endocardial and the epicardial surface for each point. Motion was quantified at

each point by computing the distance between it and the ES surface, along a line perpendicular to the surface midway between ED and ES (Fig. 2).

Displays

We displayed the perfusion and motion results using three-dimensional graphics with 24-bit true color. The triangulated LV surface was shaded using standard three-dimensional graphics techniques. A color was assigned to each LV point, and interpolated over adjacent triangles, based on the functional parameter we wished to display, so regional perfusion or motion could be visualized.

The three-dimensional LV could be simultaneously displayed in cine mode and interactively rotated. The display could be almost instantly switched between display of endocardial and epicardial surfaces, and between display of motion and perfusion.

Validations

We acquired GSPECT TRVGs from four subjects and GSPECT sestamibis from four additional subjects. MR images were obtained from all eight subjects. Boundaries were automatically detected in the GSPECT image using the methods described above. The ED and ES frames of each MR image were interactively traced. Motion calculations were performed using the previously described model for both GSPECT and MR endocardial surfaces. Motion was averaged over nine geometrically-defined regions that corresponded to the apex, and the apical and basal halves of the anterior, septal, diaphragmatic (inferior and posterior) and lateral walls of the LV. In each region, the average motion calculated from the GSPECT was compared to that computed from the MR image of the same patient.

THEORETICAL LIMITS TO ACCURACY

The accuracy of motion calculation depends upon the accuracy of the surface detection algorithm. The accuracy of perfusion quantification depends on surface detection and on the assumption that image intensity is proportional to myocardial perfusion. The method used in this study assumes that perfusion is accurately represented by the maximum image intensity between the detected endo and epicardial surface points, and that myocardial boundaries are located at the zero crossing of the second derivative of the image intensity.

Neither assumption is completely valid. Image intensity is affected not only by perfusion but also by attenuation, scatter, and the modulation transfer function (MTF) of the acquisition and reconstruction process. The MTF includes the point spread function intrinsic to GSPECT instrumentation as well as smoothing algorithms used in pre-reconstruction and reconstruction filters. Because the effect of the MTF on image intensity is nonlinear, it also modifies the locations of the zero crossings of the second derivative of image intensity. Changes in perfusion and edge point location depend on the shape of the MTF, which is often described using the parameter full width at half maximum (FWHM).

The effects of attenuation and scatter on myocardial perfusion quantification using single photon imaging are typically handled by the quantification of *relative* perfusion and the acceptance of lower values in highly attenuated cardiac regions as normal (*12*). Compensation for the point spread function is usually not performed either, since correction requires detailed knowledge not only of the MTF, but also of various physical properties of both source and noise spectra. It would be useful, however, to determine the severity of the effect of the MTF on perfusion and motion quantification.

We created a one-dimensional simulation, consisting of two adjacent gate functions (Fig. 3). This curve modeled a one-dimensional profile through the actual radionuclide activity distribution in the LV myocardial wall in a sestamibi image or a profile through the right ventricle (RV) and LV in a TRVG. This activity function was convolved with a Gaussian point spread function having a variance corresponding to the measured FWHM (14 mm) of a reconstructed point source in the center of an elliptical phantom filled with water and imaged with the PRISM camera using the same protocol and parameters as were used in the patient studies. After the convolution, the resulting curve modeled a profile through a SPECT image. The differences between the true distribution and the

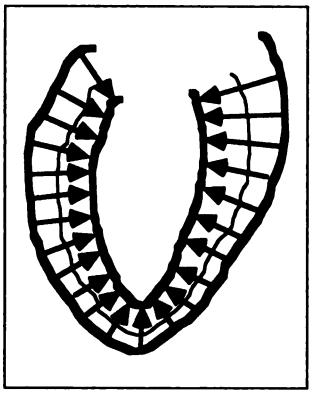

FIGURE 2. Model used for motion computation. A surface midway between end diastole and end systole is created (thin line). The intersections between a perpendicular constructed at every point on the midline surface with the ED surface and the ES surface are determined; the length of the line connecting the intersections is considered to be wall motion at that point.

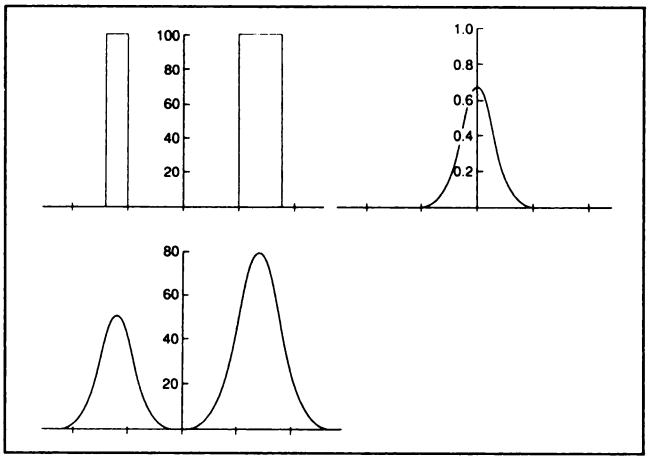

FIGURE 3. One-dimensional simulation of MTF effect on SPECT image intensity. (Top left) Simulated profile through actual sestamibi distribution in the LV. (Top Right) Simulated gaussian point spread function. (Bottom left) Result of convolution of distribution with gaussian.

image intensity included changes in the maximum intensity and the zero crossings of the second derivative.

The width and separation of the gate functions were varied; changing the widths simulated modifying wall thickness in sestamibi or chamber diameters in TRVG. Changing the separation simulated the modification of chamber diameter in sestamibi or wall thickness in TRVG. Minimum expected errors in motion calculations attributable to MTF effects could be predicted using these simulations.

If it is assumed that the chamber diameter is greater than or equal to the FWHM, then, as can be seen in Figure 4, the error in intensity persists until the widths of the gate functions are approximately twice the FWHM. This result agrees with that published in (*13*). The error in edge point location, as determined by the zero crossing, is negligible (<0.03 mm) when both the width of the gate functions and their separation are greater than the FWHM (Fig. 5).

When this is not the case, motion is likely to be underestimated. The error in motion is calculated as the error in boundary detection at end diastole minus the error at end systole. For example, myocardial wall thickness and chamber diameter average 8.5 mm and 46.0 mm at end diastole, and 18.0 mm and 27.0 mm at end systole (*14*); therefore, the error in the motion calculation in this typical situation should be equal to 2.1 mm − (0.0 mm) = 2.1 mm. This analysis is also applicable to blood-pool studies; however, in this case, the effect would be seen only along the septal wall.

Perfusion is affected more than motion by the MTF. However, we believe that our acquisition and quantification methods lessen these effects compared to more traditional perfusion acquisition and quantitation techniques. Because the images are gated, the images are less affected by temporal averaging than are ungated studies. If motion is not resolved, images represent an average of the myocardium throughout the cardiac cycle. In this study, we resolved motion with gating and used the end diastolic

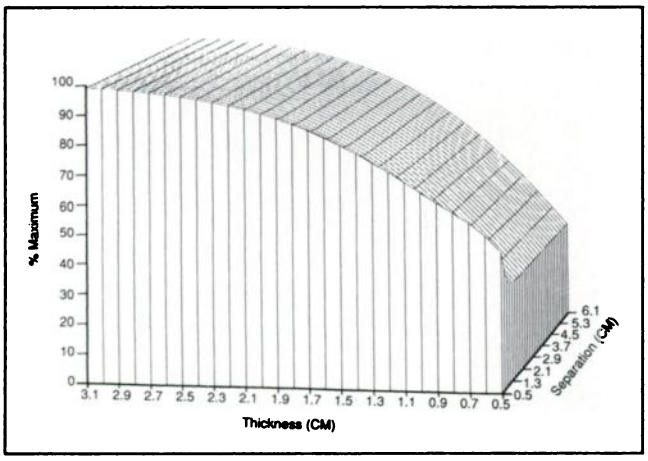

FIGURE 4. Change in maximum intensity of the simulation as width and separation of the gate functions change.

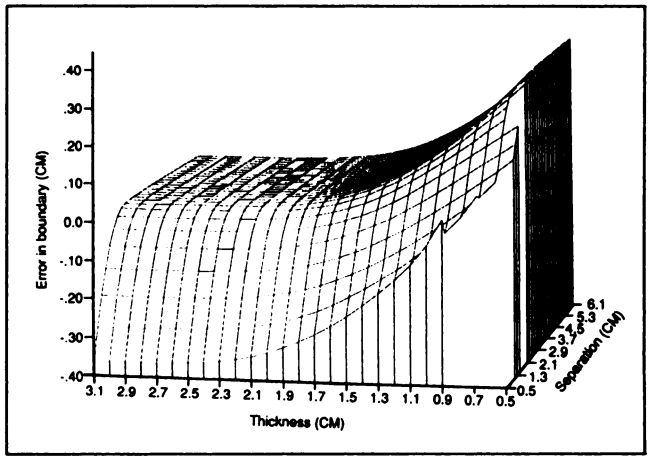

FIGURE 5. Error in surface point location as width and separation of the gate functions change.

frame for perfusion quantification. The thickness of the myocardium at end diastole in a gated study is likely to be more uniform than the thickness of the myocardium averaged over the entire cardiac cycle in an upgated study. This is especially true when hearts with regional dysynergy are considered. Therefore, the relative effect of MTF on quantification of perfusion in gated studies will be less than its effect on ungated studies.

RESULTS

Automatic motion measurements in the apical and midventricular regions of both TRVG and sestamibi images agreed well with those computed from hand-traced MR images of the same patients; the average error in these areas was 0.32 mm. The maximum error seen in these areas, 3.24 mm, occurred in the septal region of TRVG studies. Otherwise, the largest differences and standard deviations were seen in the basal regions. The mean differences and standard deviations between GSPECT and MR image motion measurements for the nine LV regions are shown in Table 1.

Figures 6 through 8 show examples of motion and perfusion computations for some specific TRVG and ses-

TABLE 1
Regional Left Ventricular Motion Errors

Region	TRVG Difference (mm) mean ± s.d.	Sestamibi Difference (mm) mean ± s.d.
Apical	−0.51 ± 2.60	−1.19 ± 2.96
Lateral	1.59 ± 2.93	0.74 ± 2.10
Basal Lateral	2.00 ± 4.47	1.58 ± 2.91
Inferior	0.07 ± 2.01	−0.97 ± 1.74
Posterior	4.28 ± 4.09	−0.48 ± 2.47
Septal	3.24 ± 2.28	0.71 ± 2.13
Basal Septal	−0.30 ± 2.77	−2.53 ± 2.93
Anterior	0.14 ± 2.50	1.87 ± 2.62
Basal Anterior	−2.12 ± 2.30	0.35 ± 4.22

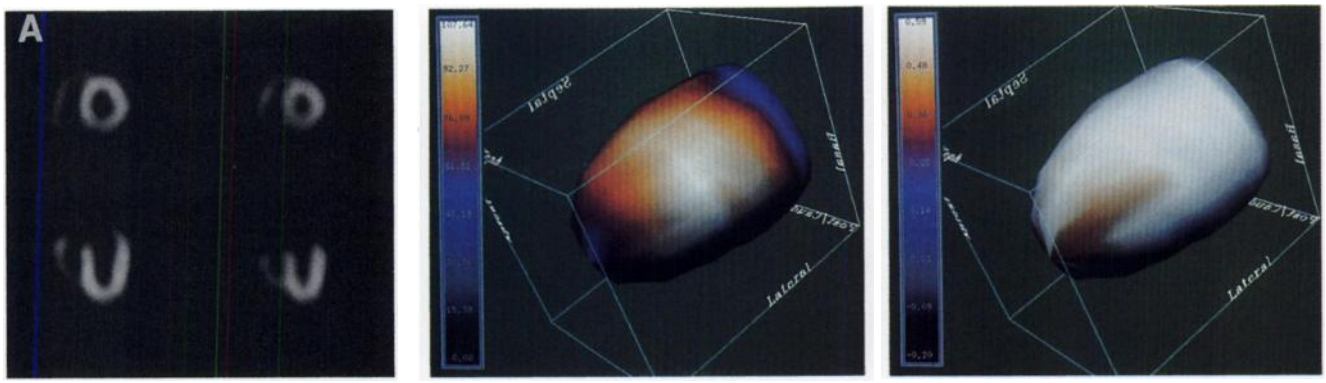

FIGURE 6. (A) ED (left) and ES (right) sections from the sestamibi image of a normal subject. Sections are mid-ventrical short-axis (top) and horizontal long-axis (bottom). (B) Antero-lateral view of the epicardial surface of the LV, color-coded for myocardial perfusion. (C) Same view of LV epicardial surface as in 6B, but color-coded for endocardial motion.

tamibi studies. Figure 6A shows ED and ES slices from the sestamibi study of a normal subject. Figure 6B shows the results of perfusion quantification color-coded onto the LV epicardial surface. Perfusion color-coding extends from black, which indicates no activity in the myocardium, to white, which indicates 100% of maximum activity in the myocardium. Note the overall uniformity of perfusion. Figure 6C shows the ED epicardial surface color-coded for motion. In these displays, motion is mapped using color such that black corresponds to the bottom of the color scale and indicates dyskinesis $\leq$ 2 mm, while white corresponds to the top of the color scale and indicates motion $\geq$ 6 mm. Motion is mapped linearly between the ends of the color scale. Note the overall white color of this normally contracting LV.

Figure 7A shows sections from the ED (left) and ES (right) frames of the TRVG from a 46-yr-old black male with an inferior infarct. Coronary angiography also indicated severe triple-vessel disease, with totally occluded right (RCA) and circumflex (Cx) coronary arteries, and a 99% stenosed left anterior descending (LAD) artery. Note the marked hypokinesis of the inferior wall of the LV. Figure 7B displays endocardial motion color-coded onto the LV at end-diastole. Note that the area of decreased motion in the inferior wall seen in Figure 7A corresponds to the area of reduced motion seen in Figure 7B and the known infarct location.

Figure 8A shows slices from the sestamibi image of a 52-yr-old white male, whose coronary angiography indicated a totally occluded LAD. Figure 8B displays the endocardial surface (with a translucent myocardium) color-coded for perfusion. In this patient, a marked reduction in perfusion is seen in the anterior/septal region; this corresponds nicely with the abnormality seen in the original images shown in Figure 8A. The same surface is seen color-coded for motion in Figure 8C. Note the relationship among the apical/septal hypokinesis seen in this view, the perfusion reduction seen in Figure 8B, and the known coronary anatomy.

DISCUSSION

These experiments show that motion and perfusion can be quantified from GSPECT studies. Motion calculations were very accurate in apical and mid-ventricular regions for both TRVG and sestamibi studies. Except in the septal area of TRVG images, mean measurements were within 0.5 pixel of the motion calculated using manually-traced

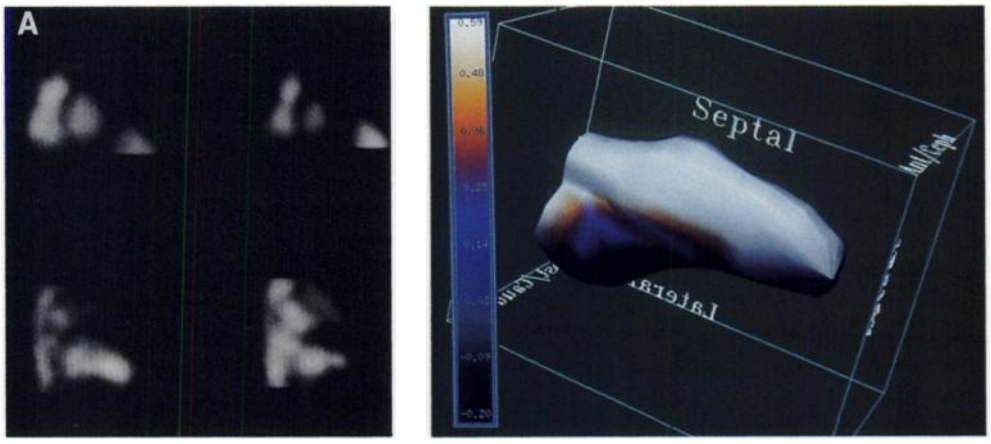

FIGURE 7. (A) ED (left) and ES (right) sections from the TRVG of a subject with an inferior infarct. Sections are basal short-axis (top) and vertical long-axis (bottom). (B) Septal view of the ED LV endocardial surface with color-coding for motion.

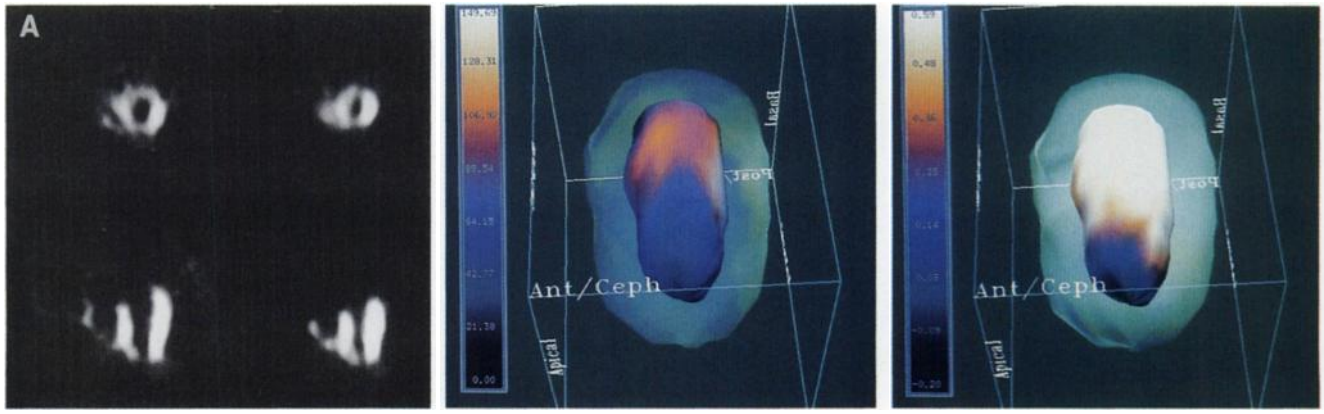

FIGURE 8. (A) ED (left) and ES (right) sections from the sestamibi image of a subject with a totally occluded LAD. Apical short-axis sections are shown on the top; horizontal long-axis sections are shown on the bottom. (B) Anterior view of the end-diastolic endocardial LV surface with a translucent myocardium, both color-coded for perfusion. (C) Same view of the LV endocardial surface, but color-coding is for endocardial motion.

MR image boundaries. Basal measurements were less precise.

The larger *positive* errors in the basal regions and the TRVG septum are due primarily to the relative lack of myocardial information in these areas. The thinner walls, including the fibrous septum near the valve planes, are affected more by the MTF. The *negative* errors seen in the basal anterior region of the TRVG studies and the basal septal regions of the sestamibi studies indicate that the detected boundaries were generally outside the true boundary. This condition may occur when a poorly-perfused region of the LV is near a normally perfused region of the RV, such as seen near the LV base. This may result in the erroneous detection of the RV boundary instead of the LV. Nevertheless, mean errors did not exceed the size of one pixel in any region, and errors in 99% of the boundary points in 5 out of 8 mid-ventricular regions were less than one pixel. Given that the resolution of the surface detector is approximately ½ pixel, these errors are quite reasonable.

In addition, note that errors in motion and perfusion quantification attributable to image degradation by the point spread function can be decreased if the system FWHM is decreased. Fortunately, new high-resolution collimators and post-processing restorative filters are becoming available for some nuclear medicine systems. These can decrease the FWHM to approximately 1 cm. As future developments further improve the resolution of SPECT imaging systems, motion and perfusion quantification should become more accurate.

However, only clinical studies can determine if our methods will be useful for diagnostic and prognostic purposes. We have performed preliminary studies on the efficacy for these methods to discriminate both perfusion and motion abnormalities with promising results (*5,6*). Previous work by other investigators has shown that quantification of perfusion in ^{201}Tl tomograms and quantification of motion in planar radionuclide ventriculograms are useful diagnostic tools. Commercially available software from a number of nuclear medicine instrumentation manufacturers provide these measurements. Qualitative studies would suggest the extension of these methods to include processing and display of additional spatial or temporal dimension may enhance their efficacy.

Current perfusion quantification techniques (*11*) are similar to those reported here, but rely on user-determined limits rather than automatic endocardial and epicardial surface detection. Displays of quantified perfusion as either two-dimensional (bulls eye) or generated geometric models (*15*), give a distorted view of the size and distribution of abnormalities.

Our motion calculation is a three-dimensional extension of the centerline method (*16*). This method assumes motion perpendicular to a boundary that is essentially halfway between the end-diastolic and end-systolic boundaries. This motion calculation does not depend on the original internal coordinate system; this is important, since the coordinate system may suffer from interoperator/intraoperator variability in its placement. The success of this method in two dimensions, described in (*17,18*), led us to implement a three-dimensional version.

Although three-dimensional displays of both TRVGs and perfusion tomograms are commercially available, most are simplistic in their design and do not quantify anything. They simply allow the user to view isocontours in three dimensions. We have developed a surface detector that does not rely on thresholds, so it neither generates "holes" in perfusion studies nor is affected by late frame count drop-off in gated studies.

CONCLUSION

The preliminary results reported here show that perfusion and motion quantification from GSPECT images can be performed giving important clinical information. Further, three-dimensional displays provide a clean and elegant method of presenting this information in an easily understandable way. Hypokinetic regions can be easily

visualized with quantitative color-coding. Three-dimensional motion also can be observed from the graphics cine display, and global and local quantitative measurements can be obtained quickly and easily. The analysis of the presented case studies demonstrates excellent correlations with known coronary anatomy and shows promise for this technique as a clinical diagnostic tool.

ACKNOWLEDGMENTS

This work was supported in part by NIH Ischemic SCOR HL17669-16.

REFERENCES

1. Corbett JR, Jansen DE, Lewis SE, et al. Tomographic gated blood-pool radionuclide ventriculography: an analysis of wall motion and left ventricular volumes in patients with coronary artery disease. *J Am Coll Cardiol* 1985;6:349–358.
2. Kahn JK, Henderson EB, Akers MS, et al. Gated and ungated tomographic perfusion imaging with technetium-99m RP-30A: comparison with Tl-201 tomography in coronary artery disease [Abstract]. *J Am Coll Cardiol* 1988;11:31A.
3. Faber TL, Stokely EM, Corbett JR. Surface detection in dynamic tomographic myocardial perfusion images by relaxation labeling. *SPIE Visual Communications and Image Processing 1988*;1001:297–301.
4. Faber TL, Kahn JK, Akers MS, Corbett JR. Automatic calculation of LV volumes and EF from gated RP-30 tomograms [Abstract]. *J Nucl Med* 1988;29:805.
5. Faber TL, McGhie AI, Akers MS, Corbett JR. Automatic quantitative assessment of motion abnormalities from gated tomographic radionuclide ventriculograms [Abstract]. *J Nucl Med* 1990;31:824.
6. Faber TL, McGhie AI, Akers MS, Corbett JR. Automatic quantification of regional myocardial perfusion and ventricular function in gated MIBI perfusion tomograms: preliminary clinical results [Abstract]. *J Nucl Med* 1990;31:859.
7. Faber TL, Stokely EM, Peshock RM, Corbett JR. A model-based four dimensional left ventricular surface detector. *IEEE Trans Med Imaging* 1991;10:321–329.
8. Smith TD, Richards P. A simple kit for the preparation of ^{99m}Tc-labeled red blood cells. *J Nucl Med* 1976;17:126–132.
9. Peshock RM, Rokey R, Malloy CM, et al. Assessment of myocardial systolic wall thickening using nuclear magnetic resonance imaging. *J Am Coll Cardiol* 1989;14:653–659.
10. Crooks LE, Barker B, Chang H, et al. Strategies for magnetic resonance imaging of the heart. *Radiology* 1984;153:459–465.
11. Garcia EV, Cooke CD, Van Train K, et al. Technical aspects of myocardial SPECT imaging with technetium-99m sestamibi. *Am J Cardiol* 1990;66:23E–31E.
12. Garcia EV, Van Train K, Maddahi J, et al. Quantification of rotational thallium-201 myocardial tomography. *J Nucl Med* 1985;26:17–26.
13. Galt JR, Garcia EV, Robbins WL. Effects of myocardial wall thickness of SPECT quantification. *IEEE Trans Med Imaging* 1990;9:144–150.
14. Feigenbaum H. *Echocardiography*, third edition. Philadelphia, PA: Lea and Febiger; 1986:550.
15. Peifer JW, Ezquerra NF, Cooke CD, et al. Visualization of multimodality cardiac imagery. *IEEE Trans Biomed Eng* 1990;37:744–756.
16. Bolson EL, Kliman S, Sheehan F, Dodge HT. Left ventricular segmental wall motion—a new method using local direction information. *Proceedings of IEEE Computers in Cardiology* 1980:245–248.
17. Sheehan FH, Stewart DK, Dodge HT, Mitten S, Bolson EL, Grown GB. Variability in the measurement of regional left ventricular wall motion from contrast angiograms. *Circulation* 1983;68:550–559.
18. Sheehan FH, Bolson EL, Dodge HT, Mathey DG, Schofer J, Woo H-W. Advantages and applications of the centerline method for characterizing regional ventricular function. *Circulation* 1986;74:293–305.